Food Hydrocolloids 137 (2023) 108422

Contents lists available at ScienceDirect

Food Hydrocolloids

journal homepage: www.elsevier.com/locate/foodhyd

Influence of processing temperature on quality attributes of meat analogues fortified with L-cysteine

Somayeh Taghian Dinani *, Noémie Allaire, Remko Boom, Atze Jan van der Goot

Food Process Engineering, Wageningen University & Research, PO Box 17, 6700, AA, Wageningen, the Netherlands

ARTICLE INFO

Keywords:
Meat analogues
L-cysteine
Processing temperature
Pea protein isolate
High-temperature shear cell
Fibrous structure

ABSTRACT

Meat analogues, mimicking the textural and sensorial properties of meat, could help consumers transition from animal-based foods to plant-based ones. However, improving the quality attributes of meat analogues, especially their textural properties is crucial to convincing more consumers to include these products in their diet. Here the effect of L-cysteine at a concentration of 0.2% in pea protein isolates (PPI) and wheat gluten (WG) blends was investigated according to the processing temperature (100, 110, 120, 130, 140, and 150 °C) in the high-temperature shear cell (HTSC). The macrostructure of fibers, as well as mechanical, microstructural, and quality attributes of products, were investigated to characterize the influence of L-cysteine on the PPI-WG blends processed at different temperatures. The results of this study showed that L-cysteine had different effects at different processing temperatures. It weakened the product structure and prevented fiber formation at processing temperatures of 100 and 110 °C. This effect was also observed at 140 and 150 °C but to a lesser extent. Conversely, at processing temperatures of 120 and 130 °C, the structure of the products with L-cysteine was stronger than those without L-cysteine, and they presented thicker fibers in visual pictures as well as the pictures obtained by scanning electron microscopy. It is concluded that L-cysteine can improve the textural properties of the meat analogues under precise processing temperatures. Thus, the potential of L-cysteine for improving the textural and quality attributes of meat analogues represents an important step towards the acceptance of a prevailing plant-based diet.

1. Introduction

In the near future, the demand for protein-rich foods will increase due to socio-economic and demographic changes (Henchion et al., 2017; OECD - FAO, 2020). Meat consumption is projected to increase by 12% over the next decade (OECD - FAO, 2020). However, animal-based foods require extensive water, land, and energy consumption and lead to high greenhouse gas emissions (de Haan, 2006; Tilman & Clark, 2014). Meat consumption also leads to ethical concerns such as animal welfare or health issues (Clark, Stewart, Panzone, Kyriazakis, & Frewer, 2017). Further, a correlation was identified between meat overconsumption and several diseases such as obesity, cancer, stroke, and chronic diseases (Bouvard et al., 2015; Cross et al., 2011; Händel et al., 2020; Micha, Wallace, & Mozaffarian, 2010). To overcome these problems, meat analogues could be attractive substitutes for meat products. Meat analogues imitate the textural, sensorial, and nutritional properties of meat, but they still differ from meat in texture and taste, which explains why many consumers still prefer meat over meat analogues (Samard & Ryu, 2019; Van Loo, Caputo, & Lusk, 2020).

Currently, the leading technology used for producing fibrous meat analogues is high moisture extrusion cooking. An alternative technology based on well-defined shear is in the development stage and is often referred to as shear cell technology (Cornet, Snel, Lesschen, van der Goot, & van der Sman, 2021; Good Food Institute, 2022). It was successfully used to make fibrous products from amongst others pea protein isolate (PPI) and wheat gluten (WG) blends (Schreuders et al., 2019). In fact, there is a growing interest in pea protein as a promising source of protein due to suitability for more moderate climates, resulting in a lower environmental impact, and it not being associated with genetically modified organisms (GMO) (Lam, Can Karaca, Tyler, & Nickerson, 2018). Furthermore, PPI is interesting for its nutritional value, availability, low allergenicity, and low cost (A. C. Y. Lam et al., 2018; Tulbek, Lam, Wang, Asavajaru, & Lam, 2017). However, pea protein yields weaker gels than soy proteins (Bildstein, Lohmann, Hennigs, Krause, & Hilz, 2008). PPI is therefore often combined with wheat gluten (WG) for its binding and structuring properties (Kyriakopoulou, Keppler, & van

* Corresponding author.
E-mail address: somayeh.taghiandinani@wur.nl (S. Taghian Dinani).

https://doi.org/10.1016/j.foodhyd.2022.108422
Received 28 September 2022; Received in revised form 14 November 2022; Accepted 16 December 2022
Available online 22 December 2022

der Goot, 2021; Schreuders et al., 2019).

Additives can be used to enhance the textural properties of meat analogues (Zhang et al., 2021) using PPI. L-cysteine as a safe cross-linking agent is a thermally unstable amino acid with a highly reactive sulfhydryl (SH) group (Li & Lee, 1996; Sameem, Khan, & Niaz, 2018), which can modify the functional characteristics and rheological properties of wheat flour extrudates (Lambert & Kokini, 2001; Li & Lee, 1996). Furthermore, Peng et al. (2022) suggested that L-cysteine affects PPI extrudates and fiber formation. These effects can be explained through considering that disulphide (SS) bonds play a major role in the structure formation of PPI extrudates (Osen, Toelstede, Eisner, & Schweiggert-Weisz, 2015). L-cysteine can initiate the inter- and intra-molecular SH/SS exchanges, increasing the inter-chain SS bonds, and resulting in a polymerization between protein monomers (N. Yang, Zhang, Li, Niu, & Yu, 2021). L-cysteine acts on the SS bonds (Li & Lee, 1998), and will affect the organoleptic properties of meat analogues such as their color and their flavor (Bredie, Hassell, Guy, & Mottram, 1997; Hui, Nip, Rogers, & Young, 2001; Li & Lee, 1996). For instance, the SH group present in L-cysteine is precursor of meaty, savory, and roasty aromas (Bredie et al., 1997; Kyriakopoulou et al., 2018). Thus, it could improve the sensorial attributes of meat analogues at appropriate concentrations. However, the different effects of L-cysteine in different protein blends are not yet clear. For instance, Taghian Dinani, van der Harst, Boom, and van der Goot (2023) and Peng et al. (2022) reported the strength of the products was increased by the addition of L-cysteine. Taghian Dinani, van der Harst, et al. (2023) investigated the effect of different concentrations of L-cysteine (0, 0.01, 0.05, 0.10, and 0.20%) on PPI and WG blends with a moisture content of 40% processed in the HTSC at 120 °C and rotation speed of 30 rpm for 15 min. They reported an improvement in the fibrousness and tensile strength of meat analogues. Peng et al. (2022) studied the effect of L-cysteine (0, 0.03, 0.06, 0.09, 0.12, 0.15%) on PPI with a moisture content of 54% processed in an extruder with five temperature zones of 40, 120, 169, 145, and 140 °C and the main temperature zone of 169 °C. They reported that increasing L-cysteine concentration from 0 to 0.09% improved the textural properties (hardness and chewiness) and fibrous structures of texturized PPI. In contrast, Koh et al. (1996), Lambert and Kokini (2001) and Li and Lee (1996, 1998) reported different results for products containing L-cysteine. Koh et al. (1996) and Li and Lee (1996, 1998) produced wheat flour extrudates containing different concentrations of L-cysteine (0–2% and 0–1.5%, respectively) with a mass flow rate of 225 g/min, screw speed of 500 rpm, total process moisture of 16%, and die temperature of 185 °C. Koh et al. (1996) reported cysteine addition decreased the expansion ratio and strands of extrudated products. Li and Lee (1996, 1998) reported the reduction of expansion ratio, bulk density, fracturability, and SS bonds and increase of gumminess, cohesiveness, hardness, chewiness, and SH bond of extrudates by increasing L-cysteine concentration. Lambert and Kokini (2001) investigated the storage modulus (G′) changes of wheat flour containing 0–0.75% L-cysteine and 25% moisture between 40 and 160 °C at 5 °C/min heating rate, 0.7% strain, and 0.75 rad/s. The results showed the maximum G′ values were around 120 °C for products containing L-cysteine and lower G′ values at temperatures less or more than this temperature. We hypothesize that these differences are related to different formulations and processing conditions, especially different processing temperatures.

Therefore, we here investigate the influence of different processing temperatures between 100 and 150 °C in the HTSC on the effect that L-cysteine has on the textural and quality attributes of meat analogues, composed of PPI and WG. The effect of temperature on L-cysteine has not been investigated yet not only in the meat analogues but also in other products. It is expected that at specific temperatures, L-cysteine may behave as a reducing agent by weakening, cleaving, or inhibiting the SS crosslinks during processing. The added L-cysteine could break initial interchain SS bonds of gluten by its SH group and, thus, could produce protein-SH or protein–SS–cysteine and reduce the protein molecular weight. Moreover, it could inhibit SS cross-linking between separate protein chains resulting in a weakened network during extrusion (Li & Lee, 1996). However, it also could improve the textural properties and the fiber structure of products (Peng et al., 2022) by creating new SS bonds between protein chains aligned to the shearing direction. Moreover, it could change quality attributes of the meat analogues, such as their color (Li & Lee, 1996) and water holding capacity at different processing temperatures. Therefore, as the effect of L-cysteine in different papers is not consistent, the effect of processing parameters, especially temperature in the protein blends containing L-cysteine should be investigated to provide a better understanding of this additive in the meat analogues.

2. Materials and methods

2.1. Materials

Commercial pea protein isolate (PPI) (NUTRALYS® S85F) and vital wheat gluten (WG) (Viten® Vital Wheat Gluten) were both obtained from Roquette Frères S.A. (Roquette Frères S.A., St. Louis, Missouri, USA). Product specifications, provided by the manufacturers, showed that WG and PPI contained a dry matter content of 92% and 92.6%, respectively. L-cysteine (97%), glutaraldehyde solution (25%), and Rhodamine B were purchased from Sigma-Aldrich (Sigma-Aldrich Co, St. Louis, Missouri, USA). Finally, ethanol (96%) was purchased from VWR International S.A.S. (VWR International S.A.S, Rosny-sous-Bois, France).

2.2. Sample preparation

Cornet, Edwards, van der Goot, and van der Sman (2020) described a general procedure for the protein blend preparation that was followed in this study with some modifications. The prepared blends without L-cysteine were composed of 60 wt% demineralized water and 40 wt% ingredients, from which 50 wt% was PPI and 50 wt% was WG. At first, PPI was mixed with demineralized water manually with a spoon. Then, the blend was covered with a plastic film to avoid moisture loss during 30 min hydration at room temperature. Next, the WG was added to the blend that was mixed by hand to obtain the final mixture before processing in the HTSC.

The prepared blends for products with L-cysteine were composed of 60 wt% demineralized water, 0.2 wt% (2000 ppm) L-cysteine, 19.9 wt% PPI, and 19.9 wt% WG. The formulation with 0.2% L-cysteine and 40% ingredients was the best in our previous research (Taghian Dinani, van der Harst, et al., 2023). First, 0.2% of L-cysteine was dissolved in demineralized water before mixing with PPI. Then, the rest of the previous procedure described for protein blends without L-cysteine was followed. Finally, protein blends without and with L-cysteine (0 and 0.2%, respectively) were produced at different HTSC temperatures (100, 110, 120, 130, 140, and 150 °C). Table 1 gives an overview of different treatments conducted. In this table, the products without and with

Table 1
Different treatments with (C) and without (N) L-cysteine at different processing temperatures in the HTSC.

Treatments	L-cysteine concentrations (%)	Processing temperature (°C)
N-100 °C	0	100
N-110 °C	0	110
N-120 °C	0	120
N-130 °C	0	130
N-140 °C	0	140
N-150 °C	0	150
C-100 °C	0.2	100
C-110 °C	0.2	110
C-120 °C	0.2	120
C-130 °C	0.2	130
C-140 °C	0.2	140
C-150 °C	0.2	150

L-cysteine are shown with N and C abbreviations. Therefore, for instance, the treatments at each temperature such as 100 °C with (C) and without (N) L-cysteine will be introduced as C-100 °C and N-100 °C.

2.3. High-temperature shear cell (HTSC) processing

The protein blends were structured in an HTSC designed at Wageningen University and Research (The Netherlands). The blends were placed in the HTSC cavity, which had been heated to the desired processing temperature (100, 110, 120, 130, 140, or 150 °C). After closing the shear cell, a constant shearing rate was applied at 39 s^{-1} (30 rpm) for 15 min. Then, the mixture was cooled down for 10 min at 25 °C without shearing (0 rpm). At the end of the process, the top cone was lifted. The product was removed from the HTSC and cooled down in a Ziplock bag at room temperature for 1 h before further analysis. Some measurements were conducted on fresh products such as a visual assessment of the fibrous structure, the tensile strength, and the color measurement. Subsequently, the products were frozen at −18 °C. All the other analyses were conducted on the frozen products. In this study, all the products were produced in triplicate.

2.4. Macrostructure

2.4.1. Product appearance and fibrous structure

The macrostructure of the processed products was evaluated with different tests. The first one examined the appearance of the sheared products obtained after processing in the HTSC and cooling down. One picture of the top side of the product was taken with the camera of a cellphone when the product was put in a white box with three sources of light-emitting diodes (DV-80SL, Falcon eyes) on the right, left, and upper sides of the box. Moreover, the fibrous macrostructure of the bent products was examined using visual pictures captured by cellphone and refractive microscopy pictures. In more detail, a piece of the product was cut, bent manually in a parallel direction to the shear flow, and put in the white box to take a picture with the cellphone. In addition, a piece of the frozen product was cut and bent similarly and placed on a spike to observe the fiber formation using refractive light microscopy (Smartzoom 5; Carl Zeiss Microscopy GmbH, Jena, Germany) with 10× magnification.

2.4.2. Tensile strength analysis

A tensile test was used to determine the strength of the samples. This test was performed with a Texture Analyzer (TA.XT Plus Connect, United Kingdom) using a static load cell of 50 N. The procedure described by Schreuders et al. (2019), Taghian Dinani, Broekema, Boom, and van der Goot (2023), and Schlangen, Ribberink, Taghian Dinani, Sagis, and van der Goot (2023) was used to measure the shear stress, shear strain and Young's modulus.

2.5. Microstructure

2.5.1. Confocal scanning laser microscopy (CSLM)

A CSLM (Stellaris 5; Leica Microsystems GmbH, Wetzlar, Germany) was used to analyze the microstructure of the samples using the procedure described by Taghian Dinani, Broekema, et al. (2023) and Taghian Dinani, van der Harst, et al. (2023).

2.5.2. Scanning electron microscopy (SEM)

SEM pictures were prepared according to the procedure described by Schreuders et al. (2022), Taghian Dinani, van der Harst, et al. (2023) and Taghian Dinani, Broekema, et al. (2023).

2.5.3. X-ray microtomography (XRT)

An XRT (GE Phoenix v|tome|x m tomographer; General Electric Go., Wunstorf, Germany) was used to study the air inclusion in the structure of the products. The procedure described by Schreuders et al. (2022) was followed with some modifications. The product was cut to 0.9 cm by 2 cm and placed in an Eppendorf tube to avoid moisture loss. A 240 kV microfocus tube with a tungsten target was applied. X-rays were produced with a current of 80 μA and a voltage of 75 kV. A GE DXR detector array was used to record the images with 2024 × 2024 pixels (pixel size 200 μm). The detector was located 815 mm from the X-ray source. The object was placed 23 mm from the X-ray source. This resulted in a spatial resolution of 6 μm. A full scan consisted of 1500 projections over 360° with 0.24° step ratio. The 1st image was skipped. The saved projection was the average of 3 images where every image was obtained using 250 ms exposure time. The GE software of Image Reconstruction (Wunstorf, Germany) was used to calculate the 3D structure via back projection. The 3D images, gained by the v|tome|x XRT, were analyzed by the software of Avizo3D 2021.2 imaging (Thermo Fischer Scientific, Waltham, Massachusetts, USA). The XRT measurement for each sample was done in duplicate. The air inclusion (void fraction) was defined as the amount of air entrapped in the structure and was calculated by dividing the air volume [cm^3] by the sample volume [cm^3].

2.5.4. Fourier transformed infrared (FTIR)

FTIR was conducted based on the procedure described by Segat et al. (2014) and Tang et al. (2021) to determine the secondary structure of the protein present in the products. Approximately 1 g of product was placed on the crystal cell of a spectrophotometer (VERTEX 70v FT-IR Spectrometer; Brucker, illerica, Massachusetts, USA) at room temperature. Then, the FTIR spectrum for each product was recorded at a resolution of 4 cm^{-1} by averaging 32 scans in the spectral range of 400–4000 cm^{-1}. Next, the secondary structure of proteins was analyzed using OriginLab software (OriginLab, Northampton, Massachusetts, USA). For that, absorbance was selected from 1600 to 1700 cm^{-1} and deconvolution was performed based on its second derivative function. In more detail, the absorbance data were plotted as a function of the wavenumber (cm^{-1}) in OriginLab software and the peak analyzer function (fit peak) was used for the peak deconvolution. For that, the baseline was subtracted based on a user-defined mode. The hidden peaks were found using positive direction, 2nd derivative method (Savitzky--Golay smooth derivative method, second polynomial order, points of the window from 7 to 15, and threshold height of 5). The fit control allowed for the adaption of the area of the peaks to the absorbance curve ($\chi^2 < 1 \times 10^5$ and $R^2 > 0.99$). The peaks in the second derivative spectra were assigned as intermolecular β-sheet (1610–1627 cm^{-1}), β-sheet (1628–1642 cm^{-1}), random coil (1643–1650 cm^{-1}), α-helix (1650–1659 cm^{-1}), and β-turn (1660–1699 cm^{-1}) (Sadat & Joye, 2020). Finally, the wavenumber and the area of each peak were extracted, and, thus, the area of each secondary structure was calculated.

2.5.5. Color properties

The color parameters of L*, a* and b* at three different places on the top surface of the products were quantified using a colorimeter (Konica Minolta model CR-400 = 410; Osaka, Japan). Then, the browning index was calculated using the following equation (Taghian Dinani & Havet, 2015):

$$BI = \frac{100}{0.17} * \left(\frac{a^{*2} + 1.75 * L^*}{5.645 * L^* + a^* - 3.012 * b^*} - 0.31 \right) \quad (1)$$

2.5.6. Water holding capacity (WHC)

The WHC was measured to find the maximum amount of water that can be bound to the product matrix. Three circular disks of 1.5 cm diameter (approximately around 1.5–2 g) were taken out of one product at approximately the same place in all the products. The disks were weighed and placed in a beaker containing around 100 ml distilled water. Then, the beakers were placed in a water bath at 50 °C for 16 h. After this, the surface water was drained gently, and samples were weighed again. The WHC (in g of water/g of sample) was derived based on the following equation (Taghian Dinani, Broekema, et al., 2023):

$$WHC = \frac{W_{ah} - W_{bh}}{W_{bh}} \times 100 \quad (2)$$

where W_{bh} and W_{ah} are the weight of the three circles from one product together before and after hydration, respectively.

2.6. Statistical analysis

In this study, a Complete Randomized Design (CRD) was performed to compare the products processed at different temperatures with (C-100, C-110, C-120, C-130, C-140, and C-150) and without L-cysteine (N-100, N-110, N-120, N-130, N-140, and N-150) using the SPSS software (Version 28.0, IBM, Armonk, NY, the USA). A descriptive Duncan's test was used to evaluate the statistical significance between products at a significant level of 95% ($P \leq 0.05$). All the results were reported as mean ± standard deviation (SD).

3. Results and discussion

3.1. Macrostructure

3.1.1. Appearance of the final products

The images of the products without (0%, N) and with L-cysteine (0.2%, C), processed at different temperatures (100, 110, 120, 130, 140, and 150 °C) in the HTSC, are presented in Fig. 1, showing the color and structural changes for different conditions. C-100 °C and C-110 °C formed a dough and not a gelled fibrous matrix. These products disintegrated when taken out of the HTSC due to their weakness. From 100 to 130 °C, the color became lighter and then darker again at higher temperatures, with or without L-cysteine. The strength and color properties are further explained in sections 3.1.3 and 3.2.6, respectively.

3.1.2. Fibrous structure investigation

Fig. 2 shows the structures in detail for the products processed. In more detail, the fibers were thin in products without L-cysteine, N-100 °C and N-110 °C. Then, the fibers became thicker with higher processing temperatures. This observation was also seen in the pictures taken by refractive microscopy, presented in the Appendix section, Fig. S1. Similar results were reported by Schreuders et al. (2019) when processing PPI-WG blends in the HTSC at different temperatures (95, 110, 120, 130, and 140 °C). In Fig. 2, the fact that N-150 °C did not completely break when folded, indicated that the product was more ductile. Thus, the fibrousness and ductility of the meat analogues were higher when the product was processed at higher temperature. A possible explanation is the stronger denaturation of the proteins under shearing at high temperatures, allowing further alignment and more (S–S) crosslinks to be formed, thus leading to a stronger network.

The same trend was visible with the products containing L-cysteine, but the extent of the effect was different, as can be observed in Fig. 2 and Fig. S1. Now, the processing temperature was more critical for products containing 0.2% L-cysteine. Addition of L-cysteine resulted in a weak dough without any visible fibers for C-100 °C and C-110 °C, while for C-120 °C and C-130 °C, the fibers were clearer and longer than the ones visible in N-120 °C and N-130 °C. For N-140 °C and C-150 °C, again elasticity was indicated by the incomplete break after folding. Therefore, both the processing temperature and the addition of L-cysteine can be used to affect the macrostructure (Figs. 1 and 2 and Fig. S1), especially the fibrousness (Fig. 2 and Fig. S1) and the mechanical properties. Interestingly, the effect of L-cysteine depended on the processing temperature. L-cysteine softened the structure at 100 and 110 °C, thereby preventing the formation of fibers. At 120 and 130 °C, it strengthened the structure and more pronounced fibers were obtained. The fiber formation with the addition of L-cysteine at 140 and 150 °C was different from that at 120 and 130 °C. The textural properties are further discussed in section 3.1.3.

3.1.3. Textural properties

Fig. 3 compares the experimental data of the shear stress [kPa] parallel (Fig. 3A) and perpendicular (Fig. 3B) to the shear flow for products without L-cysteine (0%, N) and with L-cysteine (0.2%, C) processed at different HTSC temperatures (100, 110, 120, 130, 140, and 150 °C). The shear strain and Young's modulus data of these products are shown in the Appendix section, Figs. S2 and S3, respectively. No measurements were made for C-100 °C and C-110 °C because these products did now allow to take suitable samples for this measurements.

Fig. 3 shows the tensile stress increased with increased processing temperatures in parallel and perpendicular directions, respectively. CRD statistical analysis shows that the tensile stress in both parallel and perpendicular directions to the shear flow of the tensile bars were significantly affected by different treatments ($P \leq 0.001$). The tensile stress values in the parallel direction ranged between 25.65 ± 12.77 kPa for N-100 °C and 345.71 ± 92.88 kPa for N-150 °C (Fig. 3A). Moreover, the values in the perpendicular direction ranged between 11.13 ± 2.65 kPa for N-100 °C and 178.50 ± 73.57 kPa for C-150 °C (Fig. 3B). When looking at the samples without L-cysteine, the tensile stress values from 100 to 130 °C in the parallel (Fig. 3A) and perpendicular (Fig. 3B) directions were not significantly different ($P > 0.05$). However, at higher processing temperature, the tensile stress values were significantly higher in N-140 °C and N-150 °C in comparison to N-100 °C to N-130 °C ($P \leq 0.001$) in Fig. 3A and B. In case of the products obtained with L-cysteine, the tensile stress values in Fig. 3A and B were higher for C-120 °C and C-130 °C compared to N-120 °C and N-130 °C, respectively. In contrast, for C-140 °C and C-150 °C, the tensile stress in the parallel direction was lower compared to N-140 °C and N-150 °C, respectively in Fig. 3A. In Fig. 3 B, the shear stress value in the perpendicular direction at 140 °C was lower for C-140 °C than N-140 °C, but at 150 °C, there was no significant difference.

The increase of the tensile stress with temperature, indicates an increase in the gel strength. In Fig. 3A, the reduction of shear stress for C-150 °C in comparison with C-140 °C was not statistically significant ($P > 0.05$). Similarly in Fig. 3B, there was not significant differences between N-150 °C and N-140 °C ($P > 0.05$). Therefore, this reduction could be attributed to the common sources of error such as instrumental, human, procedural, and environmental errors. Similar results were obtained by Schreuders et al. (2019) who reported that the tensile strength increased at higher temperatures for PPI-WG blends (40% dry matter including 19.5% PPI, 19.5% WG, and 1% sodium chloride). A greater denaturation due to the higher temperature increases the number of SH groups available to participate in new SS bond formation (Pietsch, Karbstein, & Emin, 2018). The proteins could denature, elongate and align in the shear direction during the heating and shearing. Then the proteins form SS bonds that sets the structure (Li & Lee, 1996).

The disintegration of the products with L-cysteine processed at 100 and 110 °C in Figs. 1–3 could show the reducing effect of L-cysteine at these temperatures, which inhibited the formation of S–S bonds. At 120 and 130 °C, the tensile stress values for both parallel and perpendicular directions were higher for C-120 °C and C-130 °C than for N-120 °C and N-130 °C. We expect here that L-cysteine may help open the existing intramolecular S–S bonds, allowing the proteins to elongate and deform better, and better expose the formed SH groups. Finally, at 140 and 150 °C, the products with L-cysteine were weaker again compared to the products without L-cysteine (Figs. 1–3). Here, the reactivity might be so high that mostly intramolecular S–S bonds were formed instead of intermolecular ones (Li & Lee, 1996). L-cysteine added to the protein blend could prevent the formation of SS bonds, which gave a weaker network. This behavior was observed at 100, 110, 140, and 150 °C (Fig. 4B). On the other hand, L-cysteine can help to improve the textural properties (Osen et al., 2015) by changing the cross-linking effect (Peng et al., 2022).

Temperature	L-cysteine concentrations	
	N (0 %)	C (0.2 %)
100 °C		
110 °C		
120 °C		
130 °C		
140 °C		
150 °C		

Fig. 1. Images of the final products obtained after HTSC treatment without (N, 0%) and with L-cysteine (C, 0.2%) processed at different HTSC processing temperatures of 100, 110, 120, 130, 140 and 150 °C.

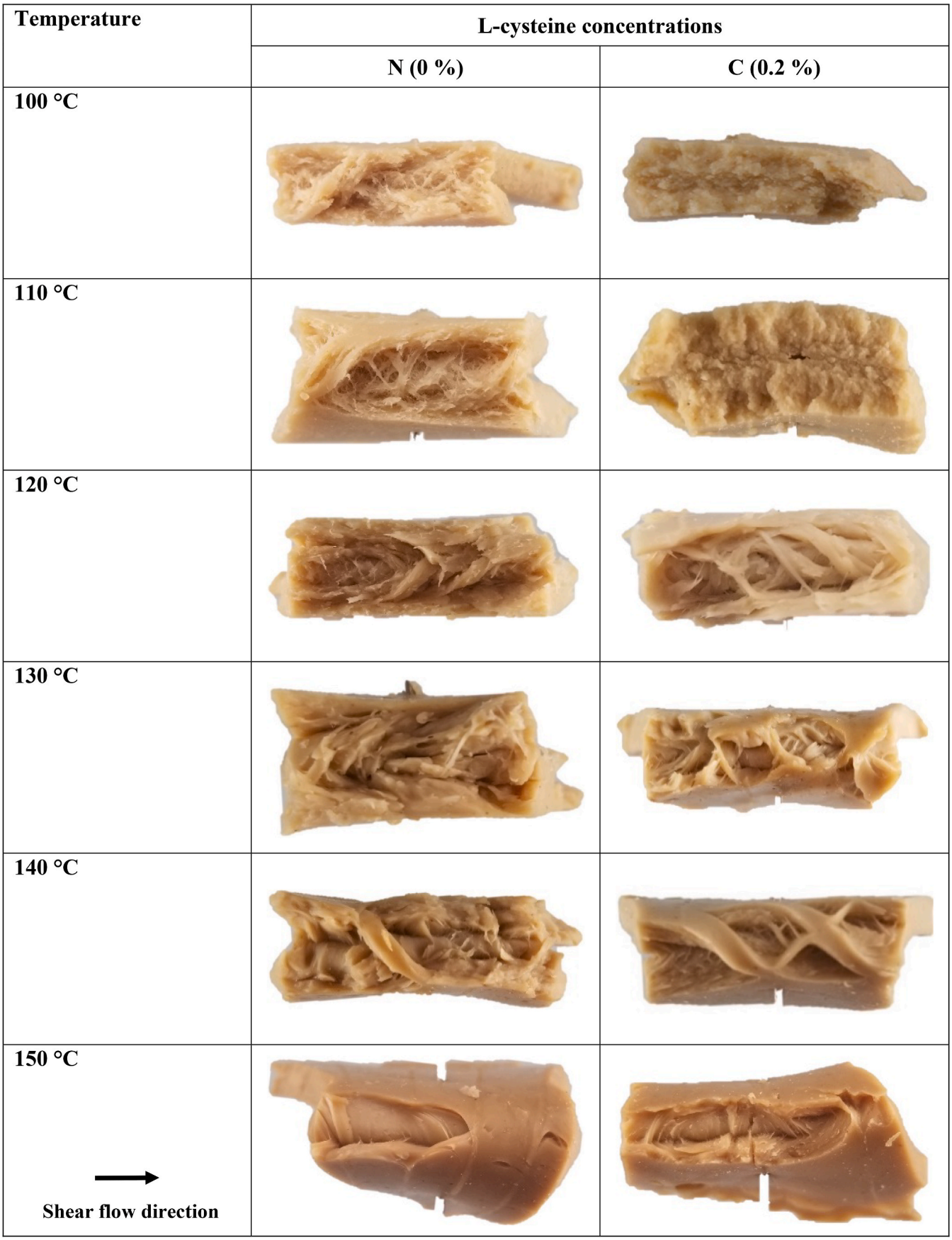

Fig. 2. Images of the fibrous macrostructure of the samples without (N, 0%) and with L-cysteine (C, 0.2%) processed at different HTSC temperatures of 100, 110, 120, 130, 140 and 150 °C.

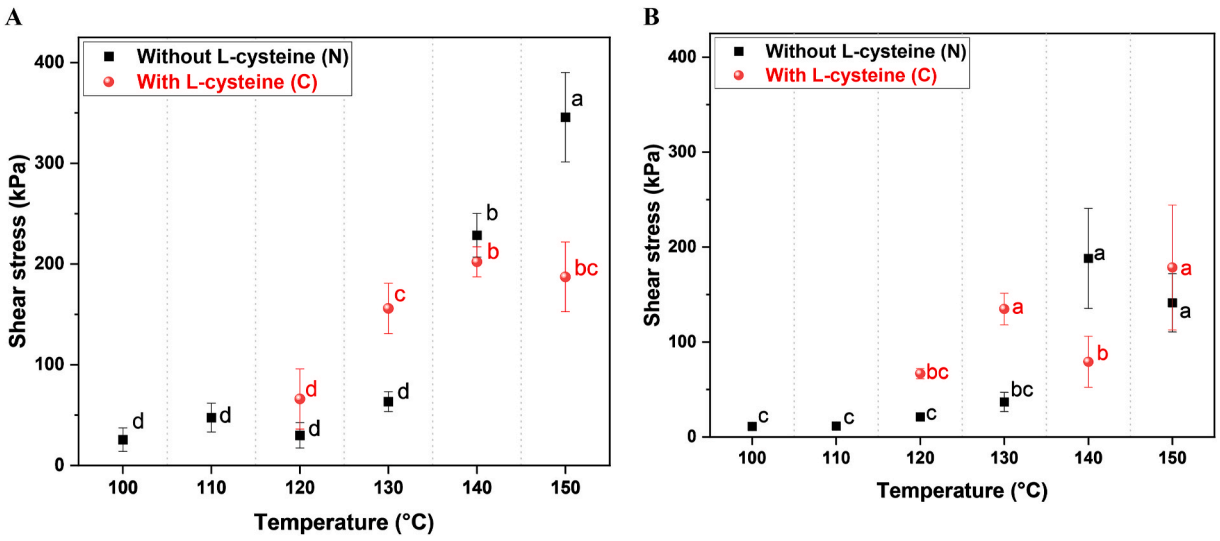

Fig. 3. Tensile stress [kPa] parallel **(A)** and perpendicular **(B)** to the shear flow direction of samples without (N, 0%) and with L-cysteine (C, 0.2%) processed at different HTSC temperatures of 100, 110, 120, 130, 140 and 150 °C. Data are shown as the mean value ± SD. Mean values with different lower-case letters are significantly different for shear stress in parallel and perpendicular directions ($P \leq 0.001$).

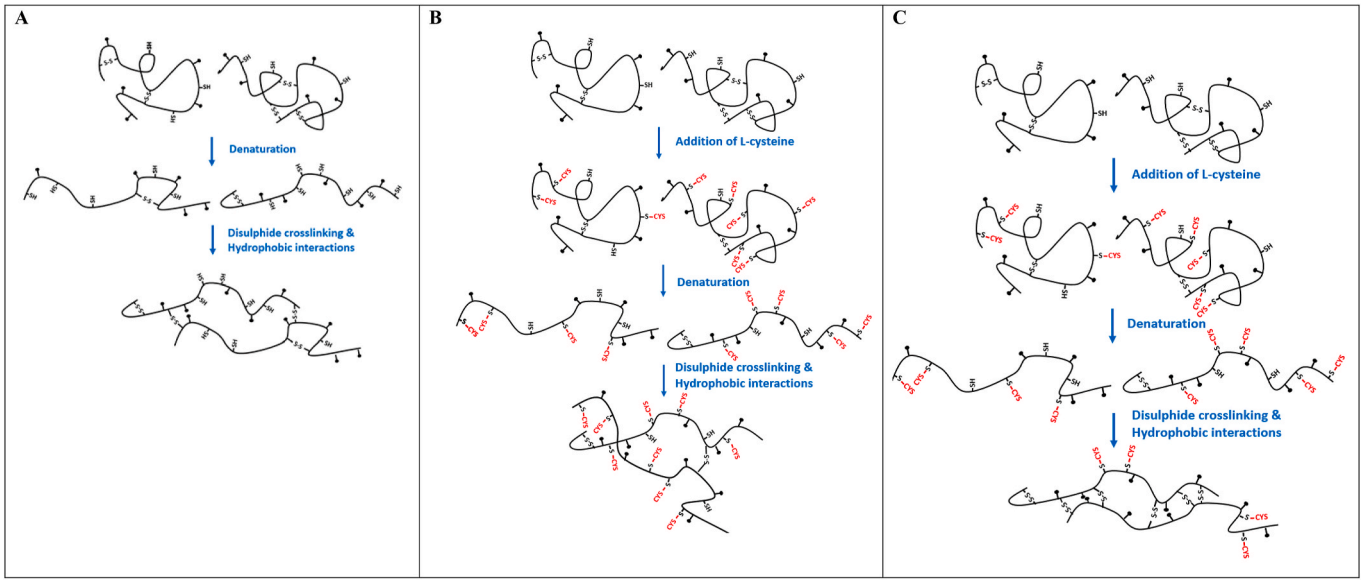

Fig. 4. Schematic diagram of a protein molecule denaturing and aligning in the direction of flow and cross-linking through disulphide and hydrophobic interaction bonds **(A)** without L-cysteine and **(B)** with L-cysteine at processing temperatures of 100, 110, 140, and 150 °C, and **(C)** with L-cysteine at processing temperatures of 120 and 130 °C. In this figure, black solid circles, SH, S–S, and CYS show the hydrophobic amino acid side chains, sulfhydryl groups, disulphide bonds, and L-cysteine, respectively.

3.2. Product microstructure

3.2.1. Confocal scanning laser microscopy (CSLM)

The distribution and the orientation of the protein domains can be studied using CSLM (Jia et al., 2021; Schreuders et al., 2019). Staining with Rhodamine B enables differentiation of different proteins from each other as well as from other constituents (Grabowska et al., 2016). Images for the C-100 °C and C-110 °C products are not available because it was not possible to take samples from the products. Fig. 5 shows for the other products that the structure of products without L-cysteine is denser with a higher processing temperature. This is confirmed by the XRT measurements of the void fraction (Figs. 7 and 8). In more detail, a dense structure containing few holes or tears can be seen for N-140 °C and N-150 °C. The high-intensity red regions visible in N-100 °C and N-110 °C were not visible anymore for products processed at a higher temperature. For N-100 °C and N-110 °C, the structures are composed of small aggregates with differences in red color intensity for some granules. Schreuders et al. (2020) demonstrated that PPI was taking up more water than WG in the PPI-WG structured products. Thus, the WG domains had a higher solids content and therefore exhibited a more intense color (Schreuders et al., 2019). Therefore, also in our system, high-intensity red regions were ascribed to the presence of a WG-rich phase.

For C-120 °C and C-130 °C, thicker fibers and holes were more aligned along the shear flow direction in comparison to N-120 °C and N-130 °C (Fig. 5). This is in agreement with the visual fibers in Fig. 2 and Fig. S1. For C-140 °C and C-150 °C, the structure appeared less compact and with more holes than N-140 °C and N-150 °C. Moreover, for C-140 °C and C-150 °C, the color intensity differences brought to light the presence of dense granules.

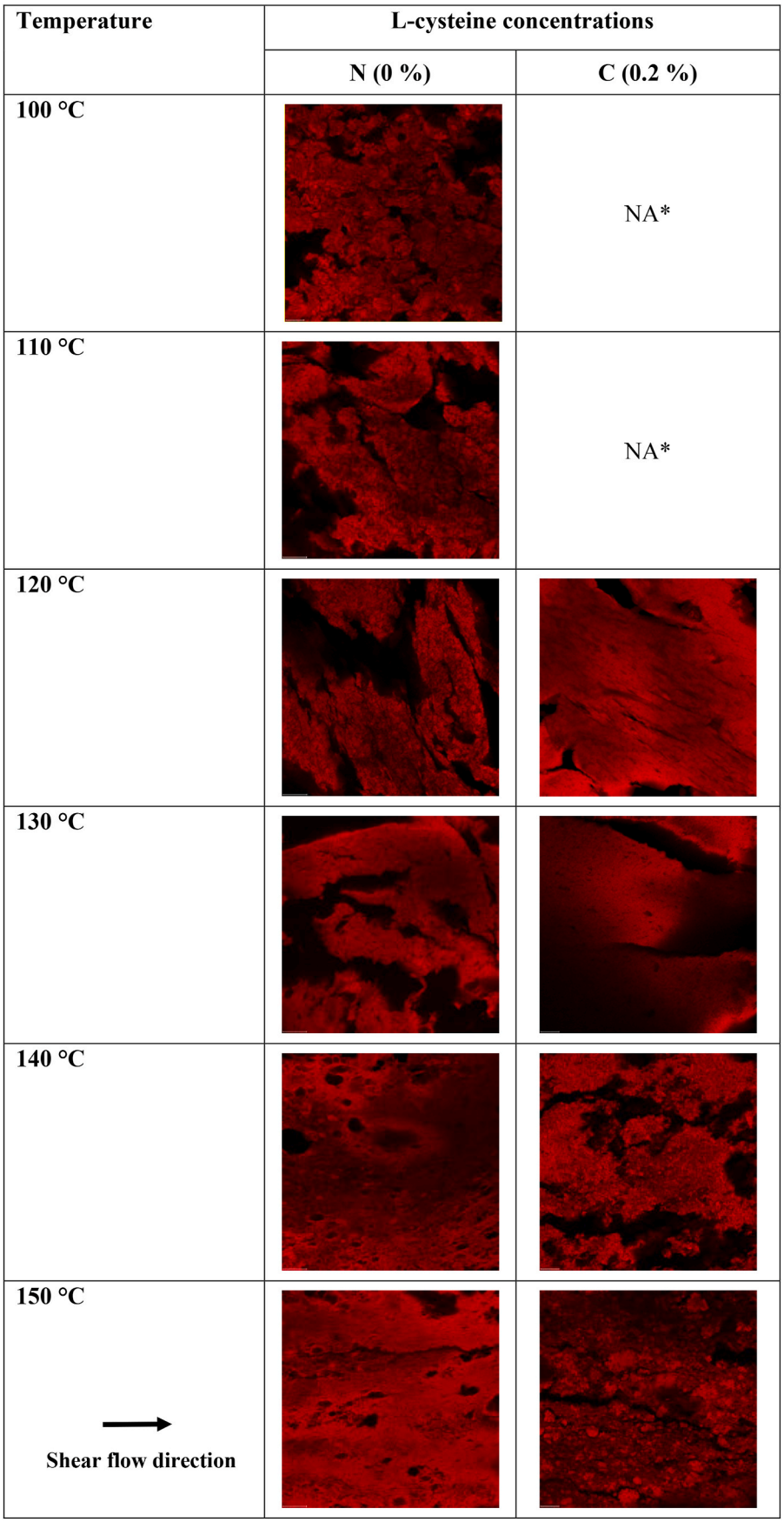

Fig. 5. CSLM images of the fluorescent channel of the product without (N, 0%) and with L-cysteine (C, 0.2%) processed at different HTSC temperatures of 100, 110, 120, 130, 140 and 150 °C. In this figure * means not available.

For N-140 °C and N-150 °C, dense structure without high-intensity red regions were found suggesting that PPI and WG phases here became more intermixed (Schreuders et al., 2019). However, the pictures of C-140 °C and C-150 °C may point out less compactness and density of the structures happening at 140 and 150 °C under the addition of L-cysteine in comparison with N-140 °C and N-150 °C. Those results suggest that the reducing effect of L-cysteine at 140 and 150 °C could lower the association of PPI and WG phases on the microstructure of C-140 °C and C-150 °C products. At those temperatures, the products containing L-cysteine present more aggregates, suggesting that the proteins are less associated compared to the products without L-cysteine. This observation is in-line with results described in the previous section (section 3.1.3).

3.2.2. Scanning electron microscopy (SEM)

Fig. 6 shows SEM images of the cross-sections from the bent (and broken) products observed at 250× magnifications. All products without and with L-cysteine presented some degree of alignment to the shear flow direction, except C-100 °C and C-110 °C. This can be nicely correlated with the visual and refractive microscopy images in Fig. 2 and Fig. S2, respectively, where all the products showed a fibrous structure except C-100 °C and C-110 °C. No degree of alignment to the shear flow direction and no fibrous structure in C-100 °C and C-110 °C products can be explained by the reducing effect of L-cysteine and the low processing temperatures of 100 and 110 °C. For the products without L-cysteine, the fibers were thin when the protein blends were processed at 100, 110, and 120 °C. At 130 °C and at higher temperatures, the fibers in the products without L-cysteine were becoming thicker, especially at 140 and 150 °C, leading to a compact structure, which can be seen in these pictures (Fig. 6).

In Fig. 6, the fibrous structure was not present in C-100 °C and C-110 °C. However, there was some alignment to the shear flow direction in N-100 °C and N-110 °C products. In contrast, thicker fibers can be observed for C-120 °C and C-130 °C compared to N-120 °C and N-130 °C. A parallel can be drawn between these results and the ones observed in Figs. 3–5. The products presenting thicker fibers in SEM pictures (Fig. 6) presented higher shear strength in Fig. 3. For instance, C-120 °C and C-130 °C had thicker fibers at microscopic and macroscopic levels (in Figs. 6 and 2, respectively) and were stronger than N-120 °C and N-130 °C (Fig. 3). Moreover, these products showed thicker fibers in CSLM pictures (Fig. 5). Thinner fibers in C-140 °C and C-150 °C compared respectively to N-140 °C and N-150 °C at the microscopic level in Fig. 5 might be again explained by the reducing effect of L-cysteine, cutting the SS bonds (Fig. 4) and weakening the structure (Fig. 3). Therefore, we suggest that the thickness of the fibers in N-140 °C and N-150 °C is correlated to the strength of the products in comparison with C-140 °C and C-150 °C.

3.2.3. X-ray microtomography (XRT)

Air bubbles are entrapped during thermo-mechanical processing. Those bubbles play an essential role in the formation of a fibrous structure (Beniwal, Singh, Kaur, Hardacre, & Singh, 2021) and anisotropy (Dekkers, Boom, & Goot, 2018; Wang, Tian, Boom, & van der Goot, 2019). Therefore, XRT was used to quantify the air fraction present in the PPI-WG blends and characterize the number and shape of the bubbles. Fig. 7 depicts the microtomographs of the solid (in purple color) and the air (in blue color) fractions of reconstructed PPI-WG products without L-cysteine (0%, N) and with L-cysteine (0.2%, C) processed at 100, 120, and 150 °C in the HTSC. It can be seen in Fig. 7 that for N-150 °C and C-150 °C, there were very few air bubbles in the products, and the products were very dense. This figure also shows that N-100 °C, N-120 °C, and C-120 °C contained a considerable amount of entrapped air bubbles. For C-120 °C, the air bubbles looked more concentrated and oriented in the shear flow direction in comparison with N-100 °C and N-120 °C (Fig. 7).

The void fraction for these XRT pictures is represented in Fig. 8. CRD statistical analysis revealed that the void fraction was significantly affected by the different treatments ($P \leq 0.001$) in Fig. 8. The void fraction values ranged between $7.67 \times 10^{-4} \pm 0.00\%$ for C-150 °C and $3.22 \pm 0.47\%$ for C-120 °C (Fig. 8). Therefore, this figure shows that C-120 °C contained the most air among all the products analyzed in Fig. 7. At the processing temperature of 150 °C, the void fraction was close to zero. These results can be linked to the observation made based on Fig. 7, where it is shown that the number of air bubbles present in the products decreased when applying a higher process temperature (Figs. 7 and 8). This observation was also made by Schreuders et al. (2019),. Our results show that the addition of L-cysteine at 120 °C increased the air fraction of the product compared to N-120 °C. This can be the reason for the thicker and more aligned fibers in this product at both microscopic (Fig. 2 and S1) and macroscopic (Figs. 5 and 6) levels compared to those in N-120 °C.

3.2.4. Protein secondary structure in FTIR spectra

The amide region band (1600-1700 cm^{-1}) in an FTIR spectrum is related to C═O stretching vibrations (Tang et al., 2021), and is the most informative to examine the secondary structures in proteins (Yao et al., 2018). Fig. 9 depicts the peak areas [%] of intermolecular β-sheets (black), β-sheets (in pink color), random coils (in yellow color), and β-turns (in blue color) in the secondary structure of the protein blends without L-cysteine (0%, N) and with L-cysteine (0.2%, C) processed at 100, 110, 120, 130, 140, and 150 °C in the HTSC.

All products presented β-turn as a secondary structure of the proteins. The values were ranging between $18.88 \pm 2.65\%$ for N-130 °C and $32.08 \pm 11.06\%$ for C-130 °C. However, the β-turn values were not significantly affected ($P > 0.05$) in this figure. CRD statistical analysis shows that the intermolecular β-sheet, β-sheet, and random coil values were significantly affected by different treatments ($P \leq 0.05$, $P \leq 0.001$, and $P \leq 0.001$, respectively).

In addition, all products showed intermolecular β-sheets as a secondary structure of the proteins. The values were ranging between $24.04 \pm 2.69\%$ for C-130 °C and $34.66 \pm 1.05\%$ for C-100 °C (Fig. 9). However, only four treatments (N-140 °C, N-150 °C, C-120 °C, and C-130 °C) were presenting β-sheet as a secondary structure and the values of these four treatments were ranged between $43.87 \pm 8.37\%$ for C-130 °C and $48.19 \pm 3.54\%$ for N-140 °C. In this figure, the products presenting some β-sheet (N-140 °C, N-150 °C, C-120 °C, and C-130 °C) did not have a random coil structure. Thus, random coils were present in other eight treatments (N-100 °C, N-110 °C, N-120 °C, N-130 °C, C-100 °C, C-110 °C, C-140 °C, C-150 °C). The random coil values in these eight treatments were ranging between $45.24 \pm 1.47\%$ for C-100 °C and $51.40 \pm 1.25\%$ for N-130 °C.

It can be concluded that the products presenting a β-sheet secondary structure of the proteins in Fig. 9 were also the ones that showed the thicker fibers in the SEM images. According to Pelton and McLean (2000), many SS bonds stabilize the β-sheet secondary structure. While the β-sheets are highly ordered, the random coils are denatured, unordered proteins. Therefore, we could expect a higher tensile strength of the products presenting around 50% β-sheet compared to the products presenting around 50% random coil in the secondary structure of the proteins. It has indeed been found that the presence of proteins with a β-sheet secondary structure resulted in a stronger, more stable and more fibrous structure (Mattice & Marangoni, 2020; Zhang et al., 2021). A parallel can be drawn with the shear stress observations (in Fig. 3). The strongest products were presenting higher shear stress in parallel and perpendicular directions (N-140 °C, N-150 °C, C-140 °C, C-150 °C, C-120 °C, and C-130 °C) in Fig. 3. These products except C-140 °C and C-150 °C had some β-sheet secondary structure in Fig. 9. Therefore, we suggest that L-cysteine at high temperatures (140 and 150 °C) destroyed the β-sheet structure and transformed it to a random coil.

In our study, α-helix was not found in any treatment. According to Beck, Knoerzer, and Arcot (2017), an extrusion process would significantly decrease the amount of α-helix present. Moreover, they suggested

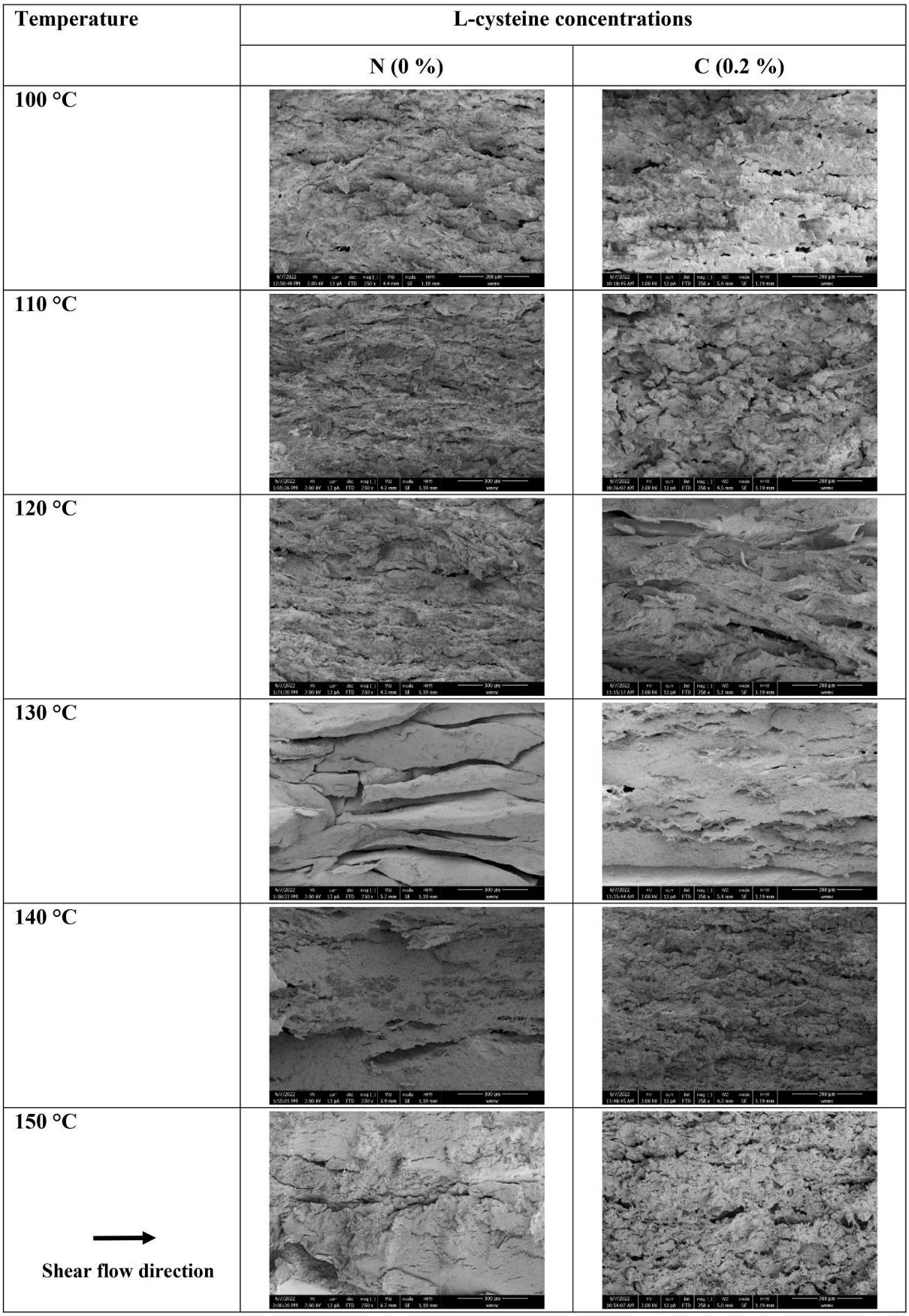

Fig. 6. Scanning electron microscopic images of cross-sections from the bent meat analogue samples without (0%) and with L-cysteine (0.2%) processed at temperatures of 100, 110, 120, 130, 140 and 150 °C at 250× magnification.

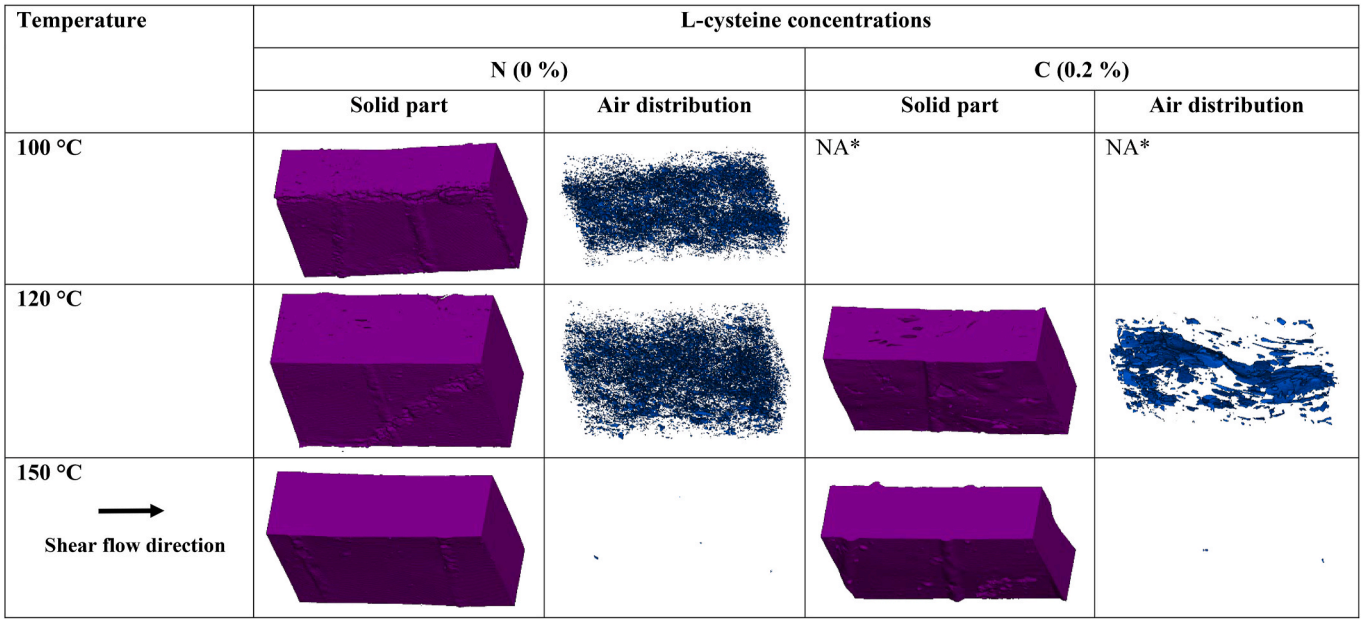

Fig. 7. X-ray microtomography images of the solid (purple) and the air (blue) fractions of a reconstructed piece of PPI-WG blend without L-cysteine (0%, N) and with L-cysteine (0.2%, C) processed at temperatures of 100, 110, 120, 130, 140 and 150 °C. In this figure * means not available. (For interpretation of the references to color in this figure legend, the reader is referred to the Web version of this article.)

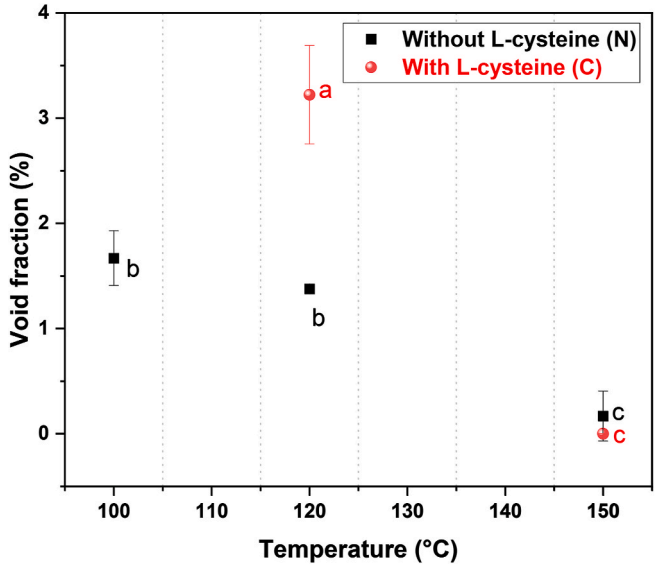

Fig. 8. Void fraction [%] (black) of PPI-WG blend without (N, 0%) and with L-cysteine (C, 0.2%) processed at temperatures of 100, 110, 120, 130, 140 and 150 °C. Data are shown as the mean value ± SD. Mean values with differently upper-case letters are significantly different for the void fraction at $P \leq 0.001$.

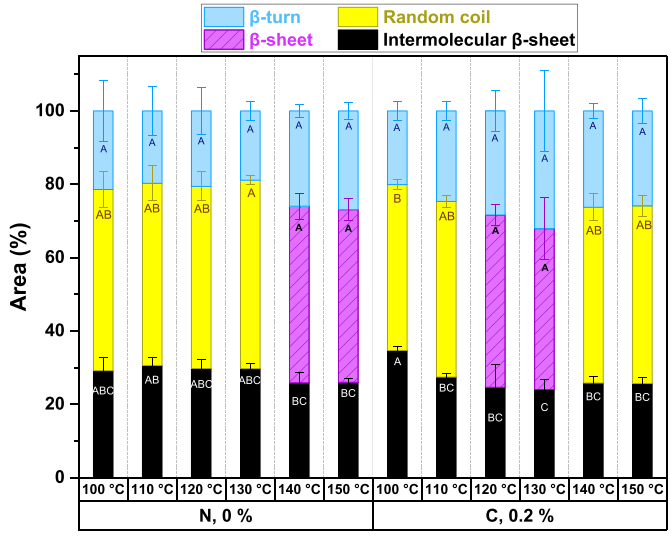

Fig. 9. Area [%] of intermolecular β-sheet (green), β-sheet (orange), random coil (yellow) and β-turn (blue) in the secondary structure of the protein blends without (N, 0%) and with L-cysteine (C, 0.2%) processed at different HTSC temperatures of 100, 110, 120, 130, 140 and 150 °C and shearing rate of 39 s^{-1}. Data are shown as the mean value ± SD. Mean values with differently upper-case letters are significantly different for intermolecular β-sheet, β-sheet, and random coil at $P \leq 0.05$, $P \leq 0.001$, and $P \leq 0.001$, respectively. The mean values for β-turn are not significantly different ($P > 0.05$). (For interpretation of the references to color in this figure legend, the reader is referred to the Web version of this article.)

that the presence of β-turns in PPI extrudates is due to the extrusion (heating and shearing) process.

3.2.5. Water holding capacity (WHC)

The WHC can be related to the sustained juiciness, or the water expelled from the product during mastication (Cornet et al., 2020, 2021). Fig. 10A compares the experimental data of the WHC [%] of products without L-cysteine (0%, N) and with L-cysteine (0.2%, C) processed at different temperatures (100, 110, 120, 130, 140, and 150 °C) in the HTSC system. In this figure, the WHC was significantly affected by different treatments ($P \leq 0.001$). The values for the WHC were between 23.48 ± 5.88% for C-140 °C and 57.49 ± 22.63% for N-100 °C in Fig. 10A. Values for C-100 °C and C-110 °C were not reported in this figure because those products disintegrated during sample preparation. Peng et al. (2022) and Li and Lee (1996) reported a reduction of WHC in their protein products upon the addition of L-cysteine (Li & Lee, 1996; Peng et al., 2022). These studies are in agreement with our results obtained for products processed at 100 and 110 °C.

Fig. 10A shows a trend in the reduction of the WHC with the increase of the processing temperature. From the tensile strength, it has been

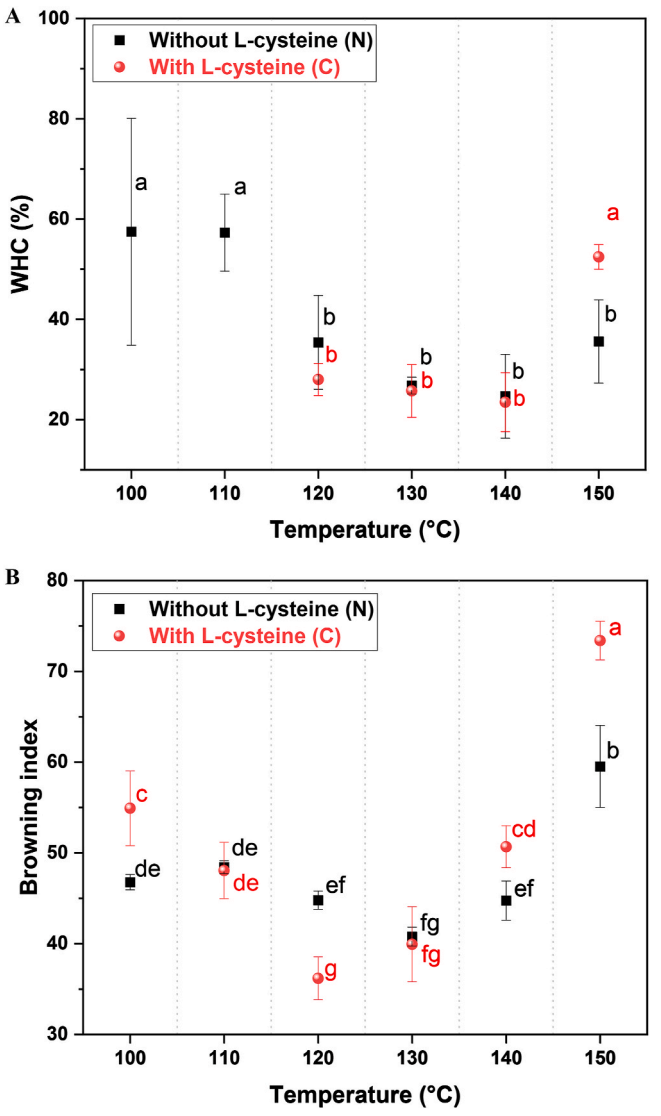

Fig. 10. (A) WHC [%] and **(B)** BI of samples without (N, 0%) and with L-cysteine (C, 0.2%) processed at temperatures of 100, 110, 120, 130, 140 and 150 C°. Data are shown as the mean value ± SD. In each figure, Mean values with different lower-case letters are significantly different ($P \leq 0.001$).

demonstrated that the increase in the temperature increased the strength (Figs. 3 and 2S) and the elasticity (Fig. 3S) of the products. Therefore, the WHC decreased as stronger structures could swallow and absorb water less (Cornet et al., 2021). It suggests the formation of additional crosslinks. It was probably for the same reasons that N-100 °C and N-110 °C had significantly higher WHC than products processed at higher temperatures. The network structure in these products should be weaker than other products processed at higher temperatures (120–150 °C) without L-cysteine or with L-cysteine processed between 120 and 140 °C. Lower shear stress in Fig. 3 and Young's modulus in Fig. S3 can confirm this argument.

The WHC value at 150 °C was higher in the product with L-cysteine (C-150 °C) than without (N-150 °C). This increase can also be the result of a decrease in the overall cross-link density in this product (Cornet et al., 2021). The cross-link density affects the elastic pressure, affecting the network deformation during swelling. Thus, the reduction of the cross-link density by L-cysteine at 150 °C could increase the physical capillarity and finally increase the amount of interaction between water and the polar sites of the products. In parallel, the decrease of the cross-link density left room for more water.

A balance of cross-link density is required. The reduction of the polymerization by L-cysteine at 100 and 100 °C yielded a structure that could not hold water. A better balance of cross-link density was available in C-150 °C in comparison to N-150 °C and other products containing L-cysteine processed at 100–140 °C. Peters, Luyten, Alting, Boom, and Van der Goot (2015) added the reducing agent dithiothreitol (DDT) which disrupts the SS bonds in whey protein gels and found that the WHC increased. Consequently, we conclude that L-cysteine can decrease the cross-link density of the products. The reduction of the cross-link density by L-cysteine is optimal at 150 °C, which results in an increased WHC value.

3.2.6. *Color properties*

Fig. 10B presents the browning index (BI) of the products without L-cysteine (0%, N) and with L-cysteine (0.2%, C) processed at different temperatures. The results of the BI were significantly affected by different treatments ($P \leq 0.001$). The results ranged between 36.18 ± 2.36 for C-120 °C and 73.39 ± 2.13 for C-150 °C. The effect of L-cysteine depended on processing temperature. Regarding the products without L-cysteine, there was no significant difference between N-100 °C, N-110 °C, N-120 °C, and N-140 °C ($P > 0.05$) or between N-120 °C, N-130 °C, and N-140 °C ($P > 0.05$). However, a large increase in the BI of the N-150 °C product can be seen in comparison to other products without L-cysteine ($P \leq 0.001$). The BI is closely related to the Maillard reaction in the products (Krishnan, Padmaja, Moorthy, Suja, & Sajeev, 2010). It is commonly accepted that at higher processing temperature more Maillard reaction will occur in food products.

The results for products with L-cysteine in Fig. 10 B were not linear with increasing the processing temperature. The BI of products containing L-cysteine from 100 °C decreased until 120 °C, after which it increased again. From 110 to 130 °C, products containing L-cysteine had lower BI values compared to the ones without L-cysteine. According to Li and Lee (1996), L-cysteine might inhibit the browning at high temperatures by two mechanisms. First of all, it will interact with the intermediate molecules found during the Maillard reaction. Second, it may dissipate free radicals formed during heating and shearing (S. Yang, Zhang, et al., 2021). The inhibitory effect of L-cysteine on Maillard reaction is most strongly visible between 100 and 120 °C. Finally, for 140 and 150 °C, the products with L-cysteine show higher browning index value. Processing with L-cysteine at high temperatures of 140 and 150 °C may expose more free amino groups for the Maillard reaction, and, thus, increase browning.

4. Conclusion

This study investigated the effects of L-cysteine at two concentrations (0 wt% (N) and 0.2 wt% (C)) in the formulation of PPI-WG blends (50/50, 40 wt%) under different processing temperatures (100, 110, 120, 130, 140 or 150 °C) in the HTSC to achieve the formation of a fibrous product with improved textural and quality attributes. The tensile strength was reduced by the addition of L-cysteine at 100 and 110 °C so much that the products disintegrated. L-cysteine increased the tensile strength at 120 and 130 °C and then reduced it again at 140 and 150 °C. Those results were correlated with the observation of no fibers for C-100 °C and C-110 °C, thicker fibers for C-120 °C and C-130 °C compared to N-120 °C and N-130 °C, and thinner fibers for C-140 °C and C-150 °C compared to N-140 °C and N-150 °C on the SEM and refractive microscopic images as well as visual pictures. This is probably related to the interplay of the reduction of the intermolecular S–S bonds, allowing better elongation and exposure for intermolecular S–S bond formation, and the general reduction of polymerization caused by L-cysteine. FTIR spectra showed the presence of β-sheet secondary structures in C-120 °C, C-130 °C suggesting a better ordered structure for those products compared to the other ones presenting a random coil secondary structure. A more compact structure with an alignment of the structure along shear flow was observed for C-120 °C and C-130 °C compared to N-

120 °C and N-130 °C in CSLM images. XRT showed a larger void fraction and stronger orientation of the air phase to the shear flow at C-120 °C. Therefore, addition of L-cysteine at appropriate temperatures may help in optimization of the structural properties of heated-sheared protein products, used for preparing plant-based meat analogues. Further research on other process parameters such as shearing time and shearing rate could provide further insight into the action of L-cysteine at different processing conditions on the textural properties.

Author statement

Somayeh Taghian Dinani: Term, Conceptualization, Formal analysis, Validation, Visualization, Supervision, Writing - Review & Editing; **Noémie Allaire**: Investigation, Formal analysis, Validation, Visualization, Writing - Original Draft; **Remko Boom**: Supervision, Funding acquisition, Writing - Review & Editing; **Atze Jan van der Goot**: Term, Conceptualization, Supervision, Funding acquisition, Writing - Review & Editing.

Declaration of competing interest

All authors declare that there is no conflict of interest.

Data availability

Data will be made available on request.

Acknowledgment

Special thanks are addressed to Jarno Gieteling, Maaike Nieuwland, Maurice Strubel, Jos Sewalt, Wouter de Groot, Martin de Wit, and Jelmer Vroom for their great technical support. Part of the presented results are obtained using X-ray tomography equipment which is owned by Shared Research Facilities and subsidized by Ministry of Economic Affairs and the province of Gelderland, The Netherlands.

Appendix A. Supplementary data

Supplementary data to this article can be found online at https://doi.org/10.1016/j.foodhyd.2022.108422.

References

Beck, S. M., Knoerzer, K., & Arcot, J. (2017). Effect of low moisture extrusion on a pea protein isolate' s expansion , solubility , molecular weight distribution and secondary structure as determined by Fourier Transform Infrared Spectroscopy (FTIR). *Journal of Food Engineering, 214*, 166–174. https://doi.org/10.1016/j.jfoodeng.2017.06.037

Beniwal, A. S., Singh, J., Kaur, L., Hardacre, A., & Singh, H. (2021). Meat analogs: Protein restructuring during thermomechanical processing. *Comprehensive Reviews in Food Science and Food Safety, 20*(2), 1221–1249. https://doi.org/10.1111/1541-4337.12721

Bildstein, M., Lohmann, M., Hennigs, C., Krause, A., & Hilz, H. (2008). An enzyme-based extraction process for the purification and enrichment of vegetable proteins to be applied in bakery products. *European Food Research and Technology, 228*(2), 177–186. https://doi.org/10.1007/s00217-008-0921-z

Bouvard, V., Loomis, D., Guyton, K. Z., Grosse, Y., Ghissassi, F. El, Benbrahim-Tallaa, L., et al. (2015). Carcinogenicity of consumption of red and processed meat. *The Lancet Oncology, 16*(16), 1599–1600. https://doi.org/10.1016/S1470-2045(15)00444-1

Bredie, W. L. P., Hassell, G. M., Guy, R. C. E., & Mottram, D. S. (1997). Aroma characteristics of extruded wheat flour and wheat starch containing added cysteine and reducing sugars. *Journal of Cereal Science, 25*, 57–63.

Clark, B., Stewart, G. B., Panzone, L. A., Kyriazakis, I., & Frewer, L. J. (2017). Citizens, consumers and farm animal welfare: A meta-analysis of willingness-to-pay studies. *Food Policy, 68*, 112–127. https://doi.org/10.1016/J.FOODPOL.2017.01.006

Cornet, S. H. V., Edwards, D., van der Goot, A. J., & van der Sman, R. G. M. (2020). Water release kinetics from soy protein gels and meat analogues as studied with confined compression. *Innovative Food Science & Emerging Technologies, 66*, Article 102528. https://doi.org/10.1016/j.ifset.2020.102528

Cornet, S. H. V., Snel, S. J. E., Lesschen, J., van der Goot, A. J., & van der Sman, R. G. M. (2021). Enhancing the water holding capacity of model meat analogues through marinade composition. *Journal of Food Engineering, 290*, Article 110283. https://doi.org/10.1016/j.jfoodeng.2020.110283

Cross, A. J., Freedman, N. D., Ren, J., Ward, M. H., Hollenbeck, A. R., Schatzkin, A., et al. (2011). Meat consumption and risk of esophageal and gastric cancer in a large prospective study. *American Journal of Gastroenterology, 106*(3), 432–442. https://doi.org/10.1038/AJG.2010.415

Dekkers, B. L., Boom, R. M., & Goot, A. J. Van Der (2018). Structuring processes for meat analogues. *Trends in Food Science & Technology, 81*, 25–36. https://doi.org/10.1016/j.tifs.2018.08.011

Good Food Institute. (2022). Introduction to plant-based meat. *Retrived September, 5*, 2022. Https://Gfi-Apac.Org/Science/the-Science-of-Plant-Based-Meat/.

Grabowska, K. J., Zhu, S., Dekkers, B. L., Ruijter, N. C. A. De, Gieteling, J., & Goot, A. J. Van Der (2016). Shear-induced structuring as a tool to make anisotropic materials using soy protein concentrate. *Journal of Food Engineering, 188*, 77–86. https://doi.org/10.1016/j.jfoodeng.2016.05.010

de Haan, C. (2006). Livestock's long shadow. Environmental issues and options. https://pdfs.semanticscholar.org/6051/608e1b9cfe1380d14b5b186a47dd2bfc6629.pdf.

Händel, M. N., Rohde, J. F., Jacobsen, R., Nielsen, S. M., Christensen, R., Alexander, D. D., et al. (2020). Processed meat intake and incidence of colorectal cancer: A systematic review and meta-analysis of prospective observational studies. *European Journal of Clinical Nutrition, 74*(8), 1132–1148. https://doi.org/10.1038/s41430-020-0576-9

Hui, Y. H., Nip, W.-K., Rogers, R. W., & Young, O. A. (2001). Chapter 4 - flavors of meat products. In *Meat science and applications*. CRC press.

Jia, W., Curubeto, N., Rodríguez-Alonso, E., Keppler, J. K., Der, A. J. Van, van der Goot, A. J., et al. (2021). Rapeseed protein concentrate as a potential ingredient for meat analogues. *Innovative Food Science & Emerging Technologies, 72*, Article 102758. https://doi.org/10.1016/j.ifset.2021.102758

Koh, Karwe, & Schaich. (1996). Effects of cysteine on free radical production and protein modification in extruded wheat flour. *Cereal Chemistry, 73*, 115–122.

Krishnan, J. G., Padmaja, G., Moorthy, S. N., Suja, G., & Sajeev, M. S. (2010). Effect of pre-soaking treatments on the nutritional profile and browning index of sweet potato and yam flours. *Innovative Food Science & Emerging Technologies, 11*(2), 387–393. https://doi.org/10.1016/j.ifset.2010.01.010

Kyriakopoulou, K., Keppler, J. K., & van der Goot, A. J. (2021). Functionality of ingredients and additives in plant-based meat analogues. *Foods, 10*(3), 600. https://doi.org/10.3390/foods10030600

Lambert, I. A., & Kokini, J. L. (2001). Effect of L-cysteine on the rheological properties of wheat flour. *Cereal Chemistry, 78*(3), 226–230. https://doi.org/10.1094/CCHEM.2001.78.3.226

Lam, A. C. Y., Can Karaca, A., Tyler, R. T., & Nickerson, M. T. (2018). Pea protein isolates: Structure, extraction, and functionality. *Food Reviews International, 34*(2), 126–147. https://doi.org/10.1080/87559129.2016.1242135

Li, M., & Lee, T.-C. (1996). Effect of cysteine on the functional properties and microstructures of wheat flour extrudates. *Journal of Agricultural and Food Chemistry, 44*(7), 1871–1880. https://pubs.acs.org/doi/full/10.1021/jf9505741.

Li, M., & Lee, T.-C. (1998). Effect of cysteine on the molecular weight distribution and the disulfide cross-link of wheat flour proteins in extrudates. *Journal of Agricultural and Food Chemistry, 46*(3), 846–853. https://pubs.acs.org/doi/full/10.1021/jf960825l.

Mattice, K. D., & Marangoni, A. G. (2020). Evaluating the use of zein in structuring plant-based products. *Current Research in Food Science, 3*, 59–66. https://doi.org/10.1016/J.CRFS.2020.03.004

Micha, R., Wallace, S. K., & Mozaffarian, D. (2010). Red and processed meat consumption and risk of incident coronary heart disease, stroke, and diabetes mellitus: A systematic review and meta-analysis. *Circulation, 121*(21), 2271–2283. https://doi.org/10.1161/CIRCULATIONAHA.109.924977

OECD - FAO. (2020). *OECD-FAO agricultural outlook 2020-2029* (pp. 162–173). Rome: OECD Publishing, Paris/FAO. https://doi.org/10.1787/1112C23B-EN

Osen, R., Toelstede, S., Eisner, P., & Schweiggert-Weisz, U. (2015). Effect of high moisture extrusion cooking on protein-protein interactions of pea (Pisum sativum L.) protein isolates. *International Journal of Food Science and Technology, 50*(6), 1390–1396. https://doi.org/10.1111/ijfs.12783

Pelton, J. T., & McLean, L. R. (2000). Spectroscopic methods for analysis of protein secondary structure. *Analytical Biochemistry, 277*(2), 167–176. https://doi.org/10.1006/ABIO.1999.4320

Peng, H., Zhang, J., Wang, S., Qi, M., Yue, M., Zhang, S., et al. (2022). High moisture extrusion of pea protein: Effect of L-cysteine on product properties and the process forming a fibrous structure. *Food Hydrocolloids, 129*, Article 107633. https://doi.org/10.1016/j.foodhyd.2022.107633

Peters, J. P. C. M., Luyten, H., Alting, A. C., Boom, R. M., & Van der Goot, A. J. (2015). Effect of crosslink density on the water-binding capacity of whey protein microparticles. *Food Hydrocolloids, 44*, 277–284. https://doi.org/10.1016/J.FOODHYD.2014.09.030

Pietsch, V. L., Karbstein, H. P., & Emin, M. A. (2018). Kinetics of wheat gluten polymerization at extrusion-like conditions relevant for the production of meat analog products. *Food Hydrocolloids, 85*, 102–109. https://doi.org/10.1016/J.FOODHYD.2018.07.008

Sadat, A., & Joye, I. J. (2020). Peak fitting applied to fourier transform infrared and Raman spectroscopic analysis of proteins. *Applied Sciences, 10*(17), 5918. https://doi.org/10.3390/app10175918

Samard, S., & Ryu, G. H. (2019). A comparison of physicochemical characteristics, texture, and structure of meat analogue and meats. *Journal of the Science of Food and Agriculture, 99*, 2708–2715. https://doi.org/10.1002/jsfa.9438

Sameem, B., Khan, F., & Niaz, K. (2018). L-Cysteine. In *Nonvitamin and nonmineral nutritional supplements* (pp. 53–58). Elsevier. https://doi.org/10.1016/B978-0-12-812491-8.00007-2.

Schlangen, M., Ribberink, M. A., Taghian Dinani, S., Sagis, L. M. C., & van der Goot, A. J. (2023). Mechanical and rheological effects of transglutaminase treatment on dense plant protein blends. *Food Hydrocolloids, 136*, Article 108261. https://doi.org/10.1016/j.foodhyd.2022.108261

Schreuders, F. K. G., Bodn, I., Erni, P., Boom, R. M., Goot, A. J. Van Der, Bodnár, I., et al. (2020). Water redistribution determined by time domain NMR explains rheological properties of dense fibrous protein blends at high temperature. *Food Hydrocolloids, 101*. https://doi.org/10.1016/j.foodhyd.2019.105562

Schreuders, F. K. G., Dekkers, B. L., Bodnár, I., Erni, P., Boom, R. M., & van der Goot, A. J. (2019). Comparing structuring potential of pea and soy protein with gluten for meat analogue preparation. *Journal of Food Engineering, 261*, 32–39. https://doi.org/10.1016/j.jfoodeng.2019.04.022

Schreuders, F. K. G., Schlangen, M., Bodnar, I., Erni, P., Boom, R. M., & Goot, A. J. Van Der (2022). Structure formation and non-linear rheology of blends of plant proteins with pectin and cellulose. *Food Hydrocolloids, 1*(124), Article 107327. https://doi.org/10.1016/j.foodhyd.2021.107327

Segat, A., Misra, N. N. N., Fabbro, A., Buchini, F., Lippe, G., Cullen, P. J., et al. (2014). Effects of ozone processing on chemical, structural and functional properties of whey protein isolate. *Food Research International, 66*, 365–372. https://doi.org/10.1016/j.foodres.2014.10.002

Taghian Dinani, S., Broekema, N. L., Boom, R., & van der Goot, A. J. (2023). Investigation potential of hydrocolloids in meat analogue preparation. *Food Hydrocolloids, 135*, Article 108199. https://doi.org/10.1016/j.foodhyd.2022.108199

Taghian Dinani, S., & Havet, M. (2015). Effect of voltage and air flow velocity of combined convective-electrohydrodynamic drying system on the physical properties of mushroom slices. *Industrial Crops and Products, 70*, 417–426. https://doi.org/10.1016/j.indcrop.2015.03.047

Taghian Dinani, S., van der Harst, J. P., Boom, R., & van der Goot, A. J. (2023). Effect of L-cysteine and L-ascorbic acid addition on properties of meat analogues. *Food Hydrocolloids, 134*. https://doi.org/10.1016/j.foodhyd.2022.108059

Tang, H., Tan, L., Chen, Y., Zhang, J., Li, H., & Chen, L. (2021). Effect of κ-carrageenan addition on protein structure and gel properties of salted duck egg white. *Journal of the Science of Food and Agriculture, 101*(4), 1389–1395. https://doi.org/10.1002/jsfa.10751

Tilman, D., & Clark, M. (2014). Global diets link environmental sustainability and human health. *Nature, 515*, 518–522. https://doi.org/10.1038/nature13959

Tulbek, M. C., Lam, R. S. H., Wang, Y. C., Asavajaru, P., & Lam, A. (2017). Pea: A sustainable vegetable protein crop. In *Sustainable protein sources* (pp. 145–164). Elsevier Inc. https://doi.org/10.1016/B978-0-12-802778-3.00009-3.

Van Loo, E. J., Caputo, V., & Lusk, J. L. (2020). Consumer preferences for farm-raised meat, lab-grown meat, and plant-based meat alternatives: Does information or brand matter? *Food Policy, 95*(July), Article 101931. https://doi.org/10.1016/j.foodpol.2020.101931

Wang, Z., Tian, B., Boom, R., & van der Goot, A. J. (2019). Air bubbles in calcium caseinate fibrous material enhances anisotropy. *Food Hydrocolloids, 87*, 497–505. https://doi.org/10.1016/j.foodhyd.2018.08.037

Yang, N., Qian, S., Jiang, Z., & Hou, J. (2021). Cysteine inducing formation and reshuffling of disulfide bonds in cold-extruded whey protein molecules: From structural and functional characteristics to cytotoxicity. *Food Chemistry, 360*. https://doi.org/10.1016/j.foodchem.2021.130121

Yang, S., Zhang, Z., Li, J., Niu, Y., & Yu, L. L. (2021). Inhibition mechanism of L-cysteine on Maillard reaction by trapping 5-Hydroxymethylfurfural. *Foods, 10*(6), 1391. https://doi.org/10.3390/foods10061391

Yao, J., Zhou, Y., Chen, X., Ma, F., Li, P., & Chen, C. (2018). Effect of sodium alginate with three molecular weight forms on the water holding capacity of chicken breast myosin gel. *Food Chemistry, 239*, 1134–1142. https://doi.org/10.1016/J.FOODCHEM.2017.07.027

Zhang, J., Chen, Q., Liu, L., Zhang, Y., He, N., & Wang, Q. (2021). High-moisture extrusion process of transglutaminase-modified peanut protein: Effect of transglutaminase on the mechanics of the process forming a fibrous structure. *Food Hydrocolloids, 112*, Article 106346. https://doi.org/10.1016/j.foodhyd.2020.106346